

Volume 11  
Number 45  
7 December 2023  
Pages 24413-25074

# Journal of Materials Chemistry A

Materials for energy and sustainability

[rsc.li/materials-a](https://rsc.li/materials-a)



ISSN 2050-7488





## PAPER

Joyce Cavalcante and Gyorgy Szekely  
Surface engineering of a superamphiphilic, self-growing  
fibrous Janus membrane prepared from mycelium



Cite this: *J. Mater. Chem. A*, 2023, **11**, 24598

# Surface engineering of a superamphiphilic, self-growing fibrous Janus membrane prepared from mycelium†

Joyce Cavalcante <sup>ab</sup> and Gyorgy Szekely <sup>\*abc</sup>

The increasing demand for effective oil–water separation materials has encouraged the exploration of sustainable and ecofriendly solutions. In this study, we investigate the surface engineering of a superamphiphilic, self-growing fibrous membrane derived from the *Pleurotus ostreatus* mycelium. A nanoporous membrane contactor facilitated the harvest of a fibrous Janus membrane by blocking the contact between the mycelium and the growth medium yet allowing nutrient transport to the mycelium. The analysis of the hydrophilicity of the membrane surface and at the mycelium–membrane interface revealed improved wettability and surface fine-tuning. The hydrophilic side was observed at the membrane–mycelium interface, whereas the hydrophobic side displayed a dense layer of closely packed fibrous hyphae. A gradient in the hypha density was revealed through Z-stack fluorescence confocal microscopy and two-dimensional segmentation analysis. The selectivity in oil–water separation was fine-tuned, which provided a sustainable and ecofriendly approach for addressing environmental challenges. The findings of this study emphasize the significance of harnessing natural compounds and self-growing fibrous mycelium as an innovative approach to surface engineering for advanced separation technologies. For the first time, we have successfully demonstrated a new application of membrane contactors for developing superamphiphilic mycelium materials.

Received 30th August 2023  
Accepted 26th October 2023

DOI: 10.1039/d3ta05220f

rsc.li/materials-a

## 1. Introduction

Bioinspired materials have drawn attention recently owing to their potential in improving membrane sustainability. Such materials replicate the functionality or structure of natural systems. Compared with conventional materials, bioinspired materials have the advantage of being sustainable and environmentally friendly because they frequently use renewable resources and are biodegradable. This factor is essential for addressing environmental challenges and reducing our ecological footprint. Nature has evolved over billions of years, leading to the development of highly optimized and effective materials. By mimicking these natural designs, scientists and engineers can create materials with enhanced properties such as

hydrophobicity<sup>1</sup> and/or amphiphilicity.<sup>2</sup> In particular, biomimetic membranes have been inspired by aquaporins,<sup>3</sup> lotus leaves,<sup>4</sup> self-assembly,<sup>5</sup> and sharkskin.<sup>6</sup>

Janus membranes are materials used for separation that have distinct characteristics on their two opposite sides. These materials have contrasting physical, chemical, or functional attributes on their surfaces, such as amphiphilicity.<sup>7</sup> Amphiphilicity refers to the dual affinity of a molecule or material toward both polar and nonpolar liquids. Superamphiphilic materials exhibit an extremely high contact angle with water (equal to or greater than 140°) on one side while having an extremely low contact angle with water (equal to or smaller than 10°) on the other side.<sup>8,9</sup> An important alternative to oil–water separation systems is the fine-tuning of a membrane surface toward superhydrophobicity and/or superhydrophilicity.<sup>10</sup>

Hydrophobic biomaterials have gained attention for their potential use in oil separation applications<sup>11,12</sup> due to their capacity to repel water while selectively adsorbing and retaining oils. Superhydrophobic biomaterials have an inherent affinity toward hydrophobic substances such as oils and hydrocarbons. They can selectively sorb and retain oils while repelling water, making them effective in oil spill remediation. The Sustainable Development Goals of the United Nations—Goal #6 on Clean Water and Sanitation, Goal #11 on Sustainable Cities and Communities, and Goal #13 on Climate Action—are all supported by adopting sustainable alternatives for oil cleanup

<sup>a</sup>Advanced Membranes and Porous Materials Center, Physical Science and Engineering Division (PSE), King Abdullah University of Science and Technology (KAUST), Thuwal 23955-6900, Saudi Arabia. E-mail: gyorgy.szekely@kaust.edu.sa; www.SzekelyGroup.com; Tel: +966128082769

<sup>b</sup>Materials Science and Engineering Program, Physical Science and Engineering Division (PSE), King Abdullah University of Science and Technology (KAUST), Thuwal, 23955-6900, Saudi Arabia

<sup>c</sup>Chemical Engineering Program, Physical Science and Engineering Division (PSE), King Abdullah University of Science and Technology (KAUST), Thuwal, 23955-6900, Saudi Arabia

† Electronic supplementary information (ESI) available. See DOI: <https://doi.org/10.1039/d3ta05220f>



materials. Fungi mycelium (Fig. 1), which is a network of thread-like structures called hyphae, has begun to attract interest as a biomaterial in recent years. Fungi mycelium can be grown into various shapes and forms, making it highly versatile for different applications. It can be molded into packaging materials,<sup>13</sup> building insulation,<sup>14</sup> and furniture.<sup>15</sup> Moreover, it can even be used as a substitute for leather.<sup>16</sup> The characteristics of fungi mycelium-based materials can be altered by adjusting their growth conditions, substrate composition, and environmental factors. As a result, its properties can be modified and tailored to fit particular requirements and applications. Mycelium materials align with the principles of the circular economy by utilizing waste streams as inputs, leaving a small environmental footprint and being compostable at the end of their life cycle.

Naturally existing biological systems offer promising solutions for developing smart surfaces with superamphiphilic properties (Fig. 1). One such instance is filamentous fungi, which generate hydrophobin, a specialized surface amphiphilic protein.<sup>17</sup> Hydrophobins play a crucial role in enabling fungi to escape their aqueous environment and facilitate the dispersal of spores through self-assembly mechanisms.<sup>18</sup> As structural elements of fungal growth, hydrophobins also play a part in how fungi interact with their surroundings. They have, for instance, been found to be crucial for aerial growth and for the attachment of fungi to solid supports.<sup>19</sup> This class of proteins presents a characteristic sequence of eight cysteine residues with conserved spacings in their primary sequence. Because of this residue spacing pattern, hydrophobins are surface-active proteins with a noncentrosymmetric arrangement of hydrophilic and hydrophobic patches.<sup>20</sup> Harnessing the properties of hydrophobins enables us to explore new avenues for creating intelligent surfaces with enhanced water-repellent characteristics.

At present, fungal mycelium-based products have attracted considerable research interest, leading to their commercialization. These remarkable materials have emerged as novel and sustainable alternatives that can replace petroleum-based products in various applications, ranging from leather

Table 1 Membrane designations and definitions according to their composition

Membrane	Definition
<b>Mycelium</b>	<i>Pleurotus ostreatus</i> mycelium
<b>PBI</b>	Nanoporous 16-wt% PBI membrane contactor
<b>PBI<sup>M</sup></b>	<b>Mycelium</b> on top of <b>PBI</b> (composite)
<b>PP</b>	Macroporous nonwoven PP membrane contactor
<b>PP<sup>M</sup></b>	<b>Mycelium</b> on top of <b>PP</b> (composite)

making,<sup>21</sup> packaging,<sup>22</sup> to building construction.<sup>23</sup> In this study, mycelium was used for the first time in nanotechnology to create a superamphiphilic self-growing Janus membrane. The membrane was inoculated on the surface of a membrane contactor, and its physicochemical characteristics were examined (Table 1). Traditionally, hydrophilic membranes have been predominantly utilized for their water permeability<sup>24</sup> and separation capabilities.<sup>25</sup> Our study, however, reveals a novel strategy that uses the hydrophilic nature of the membrane contactor to produce a unique biomembrane with exceptional superamphiphilic properties. Oil sorption tests were performed, and surface modifications in terms of topography and water–oil affinity were assessed.

This study presents a significant advancement in membrane technology by introducing the first fully biobased and self-growing Janus membrane, achieved without the use of additives or blending. We have developed an innovative interface design that not only facilitates mycelium growth but also enables easy harvesting of the resulting membrane. Furthermore, this research marks the pioneering use of hydrophobins for the development of Janus membranes. Leveraging a membrane contactor, we have successfully grown a superamphiphilic mycelium material, opening up new possibilities for membrane engineering. Importantly, this work showcases the first-ever application of mycelium in the realm of oil–water separation, offering a sustainable and efficient solution, and the resulting self-growing membrane exhibits rapid sorption characteristics. These achievements collectively highlight the

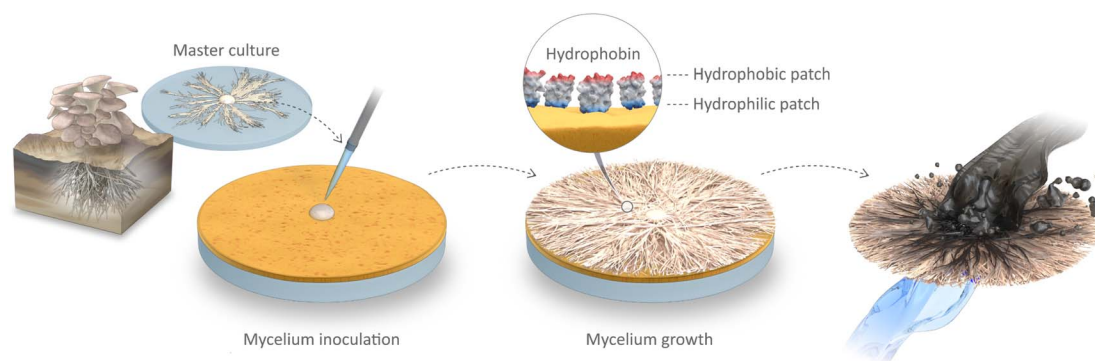


Fig. 1 Schematic illustration of the fabrication process of the superamphiphilic, self-growing fibrous membrane of *Pleurotus ostreatus* mycelium. The mycelium master culture was isolated and then inoculated on top of the membrane contactor, which allowed the mycelium membranes to grow. Through surface engineering *via* precise hydrophobin alignment, a superamphiphilic biomaterial suitable for oil–water separation was created.



groundbreaking nature of our research and its potential to revolutionize the field of membrane technology.

## 2. Results and discussion

The peak at  $3316\text{ cm}^{-1}$  in the FTIR spectrum of **Mycelium** can be attributed to the N–H stretching vibration of the amide A band in the proteins and nucleic acids and the O–H stretching vibration in phenolic compounds and  $\text{H}_2\text{O}$  (Fig. 2a). The peak at  $1640\text{ cm}^{-1}$  indicates the C=O stretching vibration in the amide I band, C=C and C=O stretching vibrations in amino acids, and N–H bending in flavonoids. The region at  $1200\text{--}900\text{ cm}^{-1}$  could be assigned to the C–O stretching vibration of the pyranose compounds in carbohydrates.<sup>26</sup> For the **PBI** membrane contactor, a broad peak was observed at  $3590\text{--}3200\text{ cm}^{-1}$ , which corresponded to the N–H stretching of the imidazole group. The distinct peaks of the benzimidazole rings were detected at  $1625\text{ cm}^{-1}$  (stretching of C=N) and  $1291\text{ cm}^{-1}$  (breathing of imidazole rings).<sup>27</sup> The **PP** membrane contactor displayed distinct peaks at  $3000\text{--}2840\text{ cm}^{-1}$  corresponding to the C–H stretching of the alkane backbone and distinct peaks at  $1473$  and  $1375\text{ cm}^{-1}$  corresponding to the C–H bending of the methyl group.<sup>28</sup> In addition to polypropylene identity peaks, mycelium-derived peaks at  $3316$  and  $1640\text{ cm}^{-1}$  were also observed for **PP<sup>M</sup>**.

Thermogravimetric analysis (TGA) results revealed that the first zone of decomposition of the **Mycelium** was in the range of  $157\text{--}320\text{ }^\circ\text{C}$  (Fig. 2b), where the decomposition of proteins, lipids, chitin, and amino acids occurred.<sup>29</sup> Above  $320\text{ }^\circ\text{C}$ , a single decomposition step occurred, which indicated the pyrolysis of cellulose and hemicellulose.<sup>30</sup> A single decomposition step at  $\sim 330\text{ }^\circ\text{C}$  was observed in case of the **PP** membrane

contactor, attributed to the thermal degradation of the covalent bonds within the polypropylene chains. The **PBI** membrane contactor exhibited a double degradation step related, attributed to the presence of the polymer backbone. The double degradation step observed in case of **PBI<sup>M</sup>** and **PP<sup>M</sup>** demonstrated the presence of various decomposition compounds originating from both the contactor and the mycelium. As observed in other works, the TGA curves did not plateau, indicating that the decomposition process was incomplete at the investigated temperature range.<sup>27,31</sup>

Differential scanning calorimetry (DSC) analysis of the **PBI** membrane contactor (Fig. 2c) revealed a single endothermic peak associated with the polymer's glass transition temperature ( $T_g$ ), which was observed at  $85\text{ }^\circ\text{C}$ . Similarly, **Mycelium** exhibited a single endothermic peak at  $70\text{ }^\circ\text{C}$ , which is its  $T_g$ . DSC analysis of **PBI<sup>M</sup>** revealed the  $T_g$  endothermic peak of the composite material at an intermediate temperature of  $77\text{ }^\circ\text{C}$  between the  $T_g$  peaks of **PBI** and **Mycelium**. **PP**, which serves as a casting support for the **PBI** membrane contactor, showed a melting temperature at  $129\text{ }^\circ\text{C}$ , where the second endothermic peak was observed. Additionally, the exothermic peak during cooling at  $118\text{ }^\circ\text{C}$  could be associated with the temperature at which **PP** crystallizes.<sup>28</sup> **PP<sup>M</sup>** exhibited distinctive transition peaks, which were attributed to the constituents of both **PP** and mycelium. An exothermic peak at  $118\text{ }^\circ\text{C}$  and an endothermic peak at  $129\text{ }^\circ\text{C}$  were identified in case of **PP**, along with an endothermic peak at  $70\text{ }^\circ\text{C}$  corresponding to **Mycelium**, which reflected the copresence of these materials.

The growth rate of mycelium was investigated from the day of inoculation, and the results are presented in Fig. 2d. Three stages of analysis were conducted: the first stage spanned the first 3 days, the second stage encompassed the following 7 days,

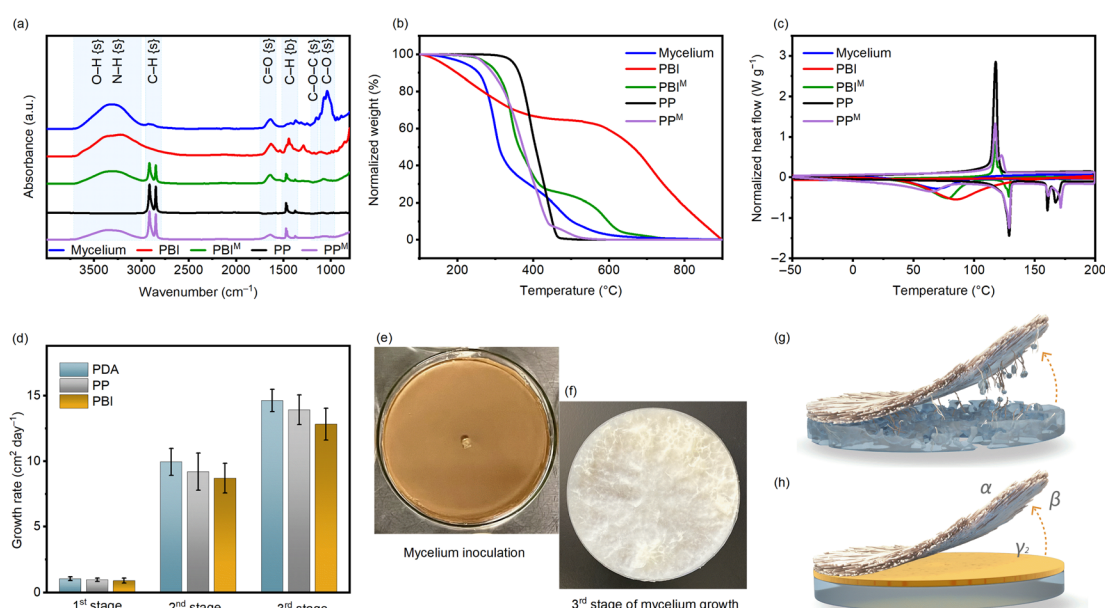


Fig. 2 (a) FTIR of the investigated membrane systems. The (s) and (b) designations correspond to the peaks caused by the stretching and bending modes, respectively. (b) TGA and (c) DSC spectra of the evaluated polymeric systems used in this study. (d) Analysis of mycelium growth rate following inoculation: after 3 days (1<sup>st</sup> stage), 7 days (2<sup>nd</sup> stage), and 21 days (3<sup>rd</sup> stage). Optical images displaying (e) mycelium inoculation on membrane contactor and (f) 3<sup>rd</sup> stage of mycelium growth. Detachment of mycelium membrane from with (g) and without (h) a nanoporous membrane contactor.



and the third stage spanned the first 21 days. Fig. S1† contains additional images of mycelium development. PDA plays a crucial role in the growth and cultivation of fungi mycelium. It provides a nutrient-rich environment that supports the growth of a variety of fungal species. At all stages of the experiment, direct contact with the growth medium (PDA) led to the fastest growth. However, when the microporous PP membrane contactor was introduced, there was a slight reduction in growth, which was primarily attributed to a decrease in nutrient transport from the PDA to the mycelium. The use of the nanoporous PBI membrane contactor resulted in the further reduction in mycelium growth rate. The mycelium cycle of growth on the PBI membrane contactor on the day of inoculation and after the third stage of growth is shown in Fig. 2e and f.

The incorporation of a membrane contactor between the growth media and the mycelium facilitates the harness of mycelium hyphae *via* the detachment of hyphae from the soft gel-like growth medium (Fig. 2g and h). We refer to the  $\alpha$  surface as the top side of the mycelium and the  $\beta$  surface as the bottom side of the mycelium, which is at the mycelium–membrane contactor interface. The top surface of the membrane contactor after the removal of the mycelium is designated as a  $\gamma_2$  surface. The membrane contactor facilitates the transfer of nutrients

from the growth medium and prevents hyphae from penetrating it. This is the first report on such an application of membrane contactors, and we encourage the community to learn more about how it can be utilized to control growth, nutrient feeding, and hyphae diameter.

In the cross-section micrographs (Fig. 3a, d, g, and j), there was no evidence of mycelium penetrating through the membrane contactor, and only hyphae were found on its surface (Fig. 3h–k). Interestingly, the surface property of the PBI membrane contactor was altered when the Mycelium was removed. The surface of the PBI became more hydrophilic, as demonstrated by the change in its wettability, and its water contact angle (WCA) decreased from  $82^\circ$  to  $47^\circ$  due to the growth of mycelium on its surface (Fig. 3b and e). Moreover, the Mycelium membrane exhibited remarkable duality in its surface characteristics: it displayed superhydrophobic behavior on its  $\alpha$  surface with a WCA of  $140^\circ$ , while forming a contrasting superhydrophilic  $\beta$  surface (WCA =  $9^\circ$ ) at the interface.

Differences in surface texture were observed and quantified through atomic force microscopy (AFM) topography measurements (Fig. 3c, f, i and l). The roughness value ( $R_a$ ) of the membrane contactor's  $\gamma_1$  surface was  $0.038 \mu\text{m}$ . Upon mycelium growth, the  $\gamma_2$  surface presented a roughness value of  $R_a =$

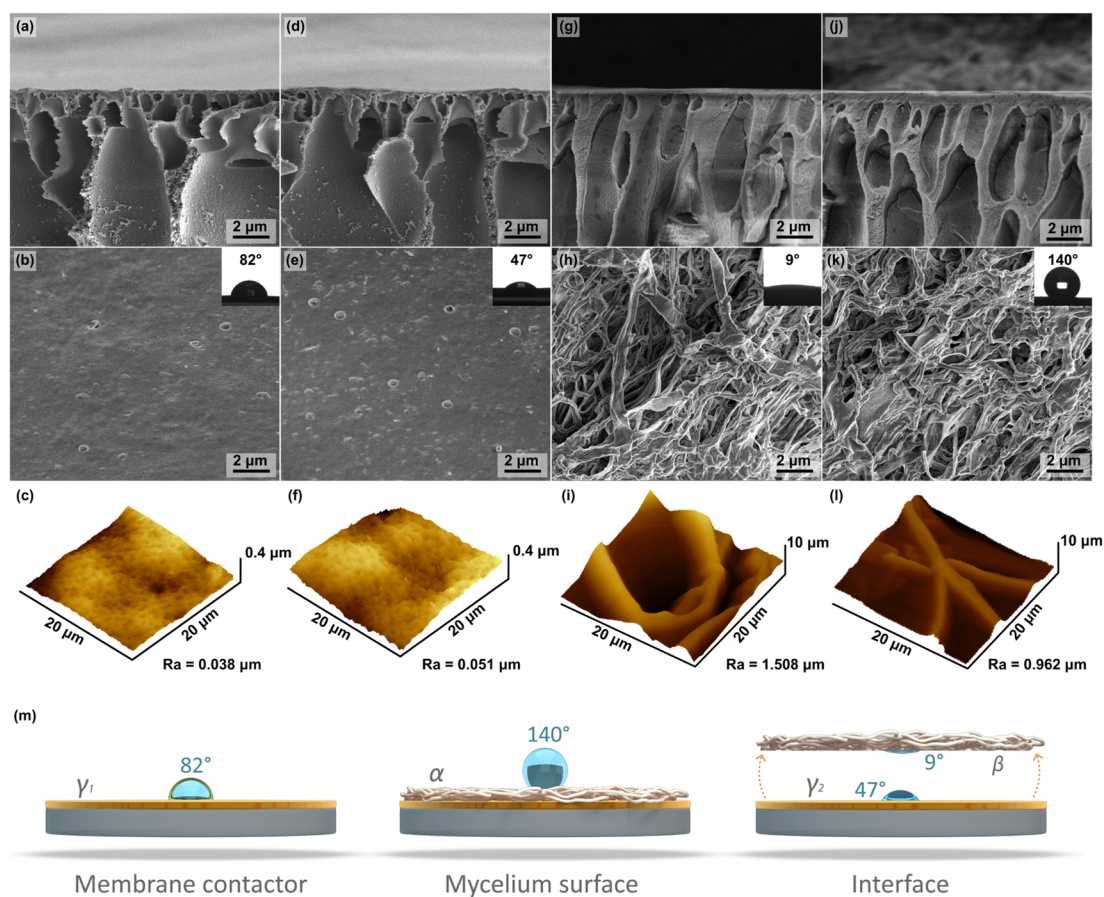


Fig. 3 (a, d, g, j) SEM cross-section, (b, e, h, k) top surface images, and (c, f, i, l) AFM three-dimensional (3D) projections of the (a, b, c)  $\gamma_1$ , (d, e, f)  $\gamma_2$ , (g, h, i)  $\beta$ , and (j, k, l)  $\alpha$  surfaces. The WCA of each surface is presented in insets. (m) Surface definitions and schematic illustration of the WCA of each investigated surface.



0.051  $\mu\text{m}$ . The surface roughness values of both sides of the mycelium membrane were measured: the hydrophilic  $\alpha$  surface displayed a roughness of  $R_a = 1.508 \mu\text{m}$ , while the hydrophobic  $\beta$  side displayed a roughness of  $R_a = 0.962 \mu\text{m}$ . The roughness values on the more hydrophilic surface were consistently higher. This phenomenon is in accordance with previous findings, demonstrating that rough surfaces enhance hydrophilicity in biofilms.<sup>32</sup> By applying the Wenzel<sup>33</sup> and Cassie–Baxter models,<sup>34</sup> we were able to conduct a quantitative analysis and obtain additional insights into these phenomena. These models provide a deeper understanding on the surface roughness and wetting characteristics of our unique mycelium–PBI. The reasons for the observed surface behavior can be attributed to two factors. First, the wetting of water onto the hydrophilic surface is encouraged by the rough surface, which may increase the effective contact area of the solid–liquid interface. Second, the rough surface offers additional adsorption sites.<sup>35</sup>

The fact that **Mycelium** is extremely amphiphilic provides evidence that our membrane surface modification method, which was inspired by nature, improved wettability because of the unique and rough fibrous microstructure of the hyphae. The

enhanced water-repellent capability of the Mycelium–membrane surface has great potential for various applications, including self-cleaning surfaces,<sup>36</sup> antifouling coatings,<sup>37</sup> and water-resistant textiles.<sup>38</sup> Our study opens a path for utilizing the intricate design principles found in nature, which include patterns, structures, and processes that have developed over millions of years to improve effectiveness, sustainability, and adaptability in the natural world. By taking inspiration from nature, we can develop useful and adaptable materials that mimic the ingenuity of nature, which leads to more efficient and sustainable solutions for various applications.

To gain a deeper understanding of the potential factors that contribute to the increase in hydrophobicity, we investigated the hydrophobin proteins in **PBI<sup>M</sup>** through optical fluorescence microscopy (Fig. 4). This analysis involved Z-stack two-dimensional (2D) (Fig. 4a and d) and three-dimensional (3D) (Fig. 4b and c) reconstructions of the top surface ( $\alpha$ ) and bottom surface ( $\beta$ ) of **Mycelium**. In a Z-stack optical fluorescence measurement, the optical path length varies according to sample density.<sup>39</sup> Greater 3D thickness and volume were produced as a result of the identification of more focal planes

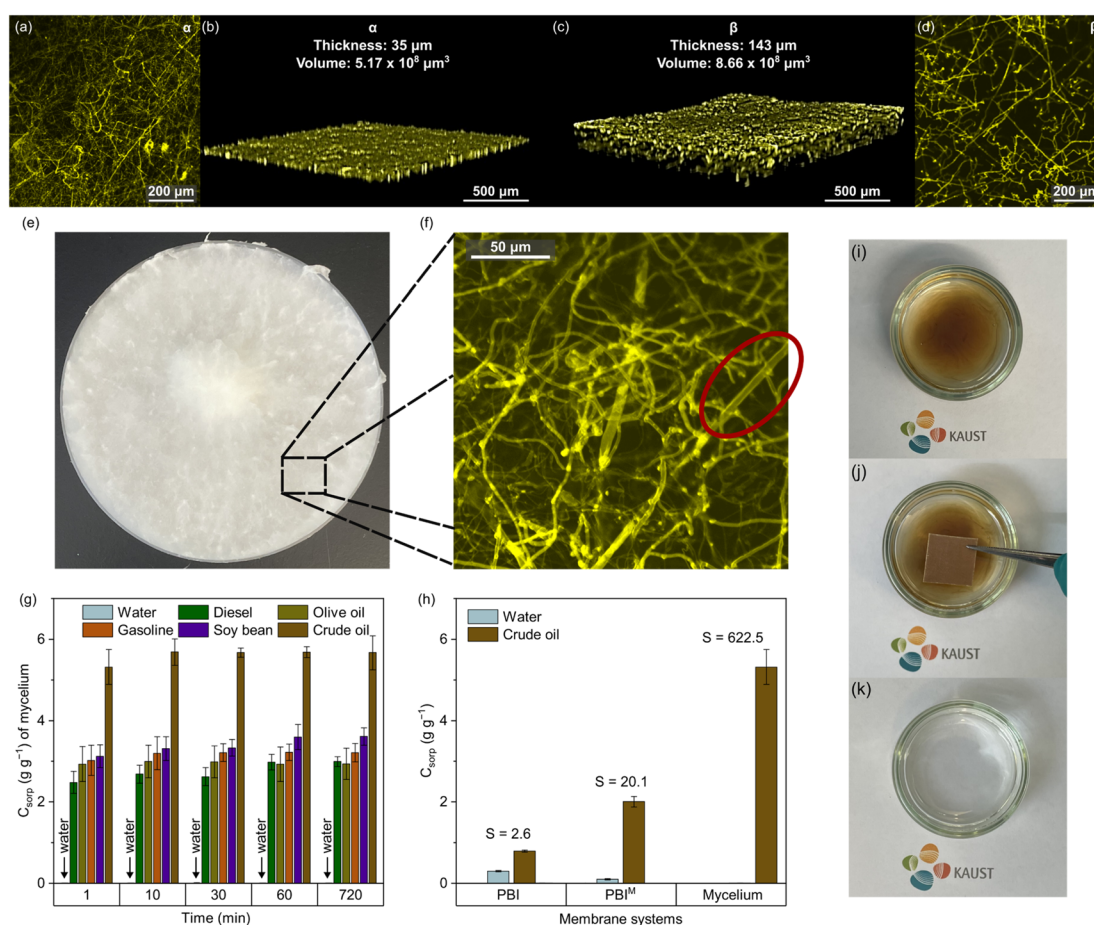


Fig. 4 (a–d) Z-stack two-dimensional and 3D hyphae distribution of the **Mycelium** membrane: (a, b)  $\alpha$  surface and (c, d)  $\beta$  surface, i.e., the interface with the PBI membrane contactor. (e) Optical and (f) fluorescence optical microscopy images of the  $\alpha$  surface of the **Mycelium** fibers. (g) Oil removal performance of **Mycelium** membrane as a function of time. Water was used in a controlled experiment to show the hydrophobic nature of our material. (h) Crude oil and water sorption after 1 min treatment using PBI, PBI<sup>M</sup>, and **Mycelium**. Optical photos of the treatment process of crude oil spill on water: (i) before, (j) during, and (k) after treatment of the crude oil spill.



due to the sparse hyphal arrangement. In contrast, a more compact hyphae arrangement produced fewer focal planes and a shorter optical path length, which produced a thinner three-dimensional Z-stack.

We found a distinct correlation between the hydrophobicity of the self-grown mycelium and the presentation of a dense and thin layer (thickness = 35  $\mu\text{m}$  and volume =  $5.17 \times 10^8 \mu\text{m}^3$ ) of tightly packed fibrous hyphae on its  $\alpha$  surface. The hydrophobic  $\alpha$  side of the **Mycelium** contrasted with its hydrophilic  $\beta$  side because the Z-stack revealed a sparse arrangement of hyphae on the interphase with the nanoporous membrane contactor (which led to a 3D thickness = 143  $\mu\text{m}$  and volume =  $8.66 \times 10^8 \mu\text{m}^3$ ). The microscopy results provided valuable visual evidence of the structural differences between the hydrophobic and hydrophilic sides of the **Mycelium** membrane, offering key insights into the mechanisms behind the observed increase in hydrophobicity.

Images of **PBI<sup>M</sup>** captured *via* Z-stack optical microscopy and labeled with Congo red fluorescence dye revealed a distinct accumulation of hydrophobin proteins on the exterior of the hyphae fibers (as shown in Fig. 4f). An optical image is also provided to show the macroscopic perspective of the mycelium fibers (Fig. 4e). In previous studies on fungi, the same staining agent was used to verify hydrophobin activity.<sup>40,41</sup> Utilizing 2D segmentation *via* Fiji (ImageJ), a gradient in the density of hyphae between the  $\alpha$  and  $\beta$  surfaces of the mycelium fibers was identified. The optical analysis (Fig. S5 and Table S2†) revealed hyphae fiber coverage of 48.2% on the  $\alpha$  surface of the **Mycelium** membrane as opposed to 39.9% on the  $\beta$  surface. The presence of surface-active hydrophobin proteins throughout the self-grown hyphae arrangement can be directly attributed to the observed gradient in fiber density. These proteins were essential in creating an amphiphilic surface, paving the way for novel insights into the surface engineering of self-growing mycelium.

A significant WCA modification, in relation to the membrane contactor, provided additional proof of the amphiphilic nature of hydrophobins. The  $\gamma^1$  surface of the pristine membrane contactor presented a WCA value of 82°, whereas the  $\gamma^2$  surface (PBI surface after mycelium growth) presented a WCA value of 47°. The pronounced modification of the PBI surface using a natural compound indicates that the surface can be fine-tuned through the hydrophobin content of mycelium. The wettability enhancement of the **PBI** surface was outstanding, as demonstrated by a 42% decrease in the WCA (Fig. 3). The decrease in WCA upon mycelium growth was a clear indication that the **PBI** surface had become hydrophilic. These findings provide additional evidence for the amphiphilic nature of the hydrophobin protein, which includes both hydrophilic and hydrophobic patches. The **Mycelium** membrane exhibited superhydrophobic behavior (WCA = 140°) on its  $\alpha$  surface, whereas it formed a superhydrophilic  $\beta$  surface (WCA = 9°) at the interface with the **PBI** membrane contactor (Fig. 3b and c). During the mycelium growth, the hydrophilic patches of the hydrophobin protein were able to attach to the surface of the membrane contactor, which oriented the hydrophobic patches of the protein in the opposite direction. The precise alignment of hydrophobins was instrumental in the creation of a superamphiphilic Janus membrane from mycelium. This alignment mechanism resulted in the

formation of a membrane with distinct hydrophobic and hydrophilic surfaces. Our findings support previous observations on hydrophobins and their application as stabilizing agents for foams and emulsions.<sup>42</sup> We showed how the unique and versatile properties of mycelium can be used as effective surface engineering tools, offering exciting opportunities for designing innovative materials with tailored wetting behavior.

Our developed composite materials are not well-suited for high-pressure applications, which led us to emphasize its potential for oil sorption and conduct relevant sorption tests. In a qualitative assessment, we found that the material exhibits excellent foldability; however, it lacks the necessary stability for tension pulling. These findings underscore its unique attributes, making it a promising candidate for specific applications where its mechanical limitations are less critical, such as in oil sorption and related environmental remediation tasks.

Amphiphilic materials have demonstrated considerable potential for efficient oil–water separation.<sup>43–45</sup> These materials possess both hydrophobic (water-repelling) and hydrophilic (water-attracting) surfaces, allowing them to selectively adsorb or repel oil and separate it from water. Janus structures enhance the efficiency of the oil–water separation processes since superamphiphilic materials create a stable interface between the oil and water phases. This selective affinity enables the material to adsorb oil onto its hydrophobic surfaces while repelling water away from these surfaces. For all oil types, including olive oil, soybean oil, diesel, gasoline, and crude oil, the sorption kinetics of our materials showed rapid oil-uptake behavior (Fig. 4g), with no discernible variation in oil sorption after the first minute of treatment. In particular, within the first minute of water treatment, the **Mycelium** membrane reached its maximum sorption capacity. According to Fig. 4h, the presence of **Mycelium** caused a 152% increase in the sorption of crude oil and a 67% decrease in water-uptake behavior in case of **PBI<sup>M</sup>** when compared with the pristine **PBI**. Oil–water selectivity (S) values, which measure the material's preference for adsorbing oil molecules over water molecules, provide a more precise quantification of this behavior. **PBI** demonstrated an S of 2.6, while **PBI<sup>M</sup>** achieved S of 20.1. Remarkably, **Mycelium** displayed a remarkable S of 622.5, demonstrating a considerably higher affinity for oil adsorption over water adsorption. Janus membranes previously reported in the literature displayed a considerably lower selectivity coefficient of 4.05.<sup>46</sup> The optical photos depict the conditions before, during, and after the treatment process, showing the sequential stages of treating crude oil spillage on water (Fig. 4i–k). Our findings present new opportunities for the use of mycelium-based materials in oil–water separation. We created the first Janus membrane for oil–water separation owing to the amphiphilic properties of hydrophobins. This membrane has a superhydrophobic surface on one side and a superhydrophilic surface on the other.

As PP is widely used in oil spill remediation,<sup>47,48</sup> we investigated its surface modification and potential oil-uptake enhancement using mycelium. Compared with the original **PP**, **PP<sup>M</sup>** showed a significant change in oil and water sorption (Fig. S7†). When compared with the results obtained using the microporous **PP** membrane contactor, mycelium was found to be responsible for an unprecedented 445% increase in crude oil



sorption and a 99.6% decrease in water sorption. We took advantage of the unique wetting behavior of mycelium, which allows for the selective repulsion of water while attracting and retaining oil. The coated  $\text{PP}^{\text{M}}$  demonstrated a remarkable selectivity of 388.6, compared to  $\text{PP}$ 's selectivity of 0.2. The reason for the remarkably higher selectivity of the composite  $\text{PP}^{\text{M}}$  compared to  $\text{PP}$  lies in the presence of a superamphiphilic mycelium Janus membrane in  $\text{PP}^{\text{M}}$ . The superhydrophobic component of the Janus coating attracts and adsorbs oil molecules effectively due to their similar nature. The presence of the Janus mycelium membrane creates a stable interface between the oil and water phases. This interface minimizes the possibility of oil droplets coalescing and re-entering the water phase, thus maintaining effective separation. The high selectivity that was achieved can be used to create cutting-edge separation materials for various oil–water mixtures, such as those used for wastewater treatment, oil spill cleanup, or industrial processes that require oil–water separation. In addition to offering a more environmentally friendly and sustainable approach, the improved performance of this material in oil–water separation also demonstrates the potential of using natural substances such as *Pleurotus ostreatus* fungi mycelium to address urgent environmental challenges. Thus, this material holds promise for contributing to the development of more efficient and environmentally friendly oil–water separation technologies.

### 3. Conclusions

Our study offers a pioneering understanding of how to use a PBI membrane contactor material for harnessing its inherent hydrophilic properties to promote the self-growth of a superamphiphilic membrane. The mycelium material exhibited a superhydrophilic contact angle of  $9^\circ$  on its  $\alpha$  surface and a superhydrophobic contact angle of  $140^\circ$  on its  $\beta$  surface, leading to an oil–water selectivity value of 622.5 and oil sorption capacity of  $5.3 \text{ g g}^{-1}$ . This is the first instance in which the hydrophilic properties of a membrane material have been successfully used to obtain superamphiphilic fibrous membrane made of mycelium. The hydrophilicity of the PBI membrane was also fine-tuned upon mycelium growth, ranging from a WCA of  $82^\circ$  on its  $\gamma_1$  surface to  $47^\circ$  on its  $\gamma_2$  surface. Overall, our study demonstrates the untapped potential of using the hydrophilicity of a membrane contactor as a useful tool in creating separation materials. This finding advances our understanding of interfacial science and paves the way for innovative applications in various industries, including coatings, materials science, and biomimetics. Even though the field of fungi mycelium-based biomaterials is still developing, it holds great promise for innovative and sustainable solutions across a range of industries, including packaging, construction, textiles, and liquid separation systems. A promising avenue for future studies lies in the potential regulation of pore size and porosity within mycelium-based Janus membranes. This critical aspect of membrane engineering can be finely tuned through various methods and factors, including pressing techniques, thermopressing, inoculation parameters, and the selection of specific fungal mycelium strains as well as membrane contactors. By strategically

manipulating these variables, researchers can tailor the membrane's structural characteristics to align with the specific demands of various applications. This ability to control pore size and porosity holds great promise for optimizing the performance of mycelium-based Janus membranes in diverse fields such as filtration, separation, and environmental remediation. Exploring these avenues further can significantly enhance the versatility and efficiency of these innovative biomaterials. The properties and performance of *Pleurotus ostreatus* mycelium materials can be enhanced through further research and development.

## 4. Experimental

### 4.1. Membrane contactor fabrication

A commercial 26-wt% polybenzimidazole (PBI) solution was diluted in *N,N*-dimethylacetamide (DMAc) using a Stovall Low Profile Roller by Stovall Life Science until a homogeneous 16-wt% dope solution was obtained. To eliminate air bubbles, the solution was shaken inside an IKA KS 3000 I control incubator for 1 day at  $40^\circ\text{C}$ . Using an Elcometer 4340 film applicator and a  $200 \mu\text{m}$ -thick casting knife, the dope solution was cast on a porous nonwoven Novatexx 2471 polypropylene (PP) flat sheet at a casting speed of  $3 \text{ cm s}^{-1}$ . Phase inversion was conducted in a coagulation bath with deionized water at  $20^\circ\text{C}$  for 24 h. The resulting membrane contactors were stored in water that contained 1-vol% ethanol to prevent microbial and fungal growth. The contactors were later used as a nanoporous interlayer to aid in the growth of mycelium. Although the membrane described above has been widely utilized as a nanofiltration membrane, this is the first instance of it being employed as a membrane contactor.<sup>49–51</sup>

### 4.2. Mycelium–membrane fabrication

Fresh oyster mushrooms were purchased from the local supermarket and used as the source for isolated colonies of *Pleurotus ostreatus*. To create master cultures, conidia (5 mm-diameter spores) from internal tissue were directly plated onto commercial PDA in 90 mm Petri dishes purchased from VWR Chemicals. Parafilm was used to seal Petri dishes, and master cultures were grown for 7 days at  $25^\circ\text{C}$  in the dark. The absence of light maintained vegetative growth, which prevented the emergence of asexual reproduction structures,<sup>52</sup> thereby preserving a mycelium made up only of intertwined hyphae. The mycelium in the plate showed radial development under these conditions. With the help of an inoculation needle and  $5 \text{ mm}^2$  of mycelium from the plate's margins, the isolated colonies were reproduced into subcultures. Mycelia were placed inversely on a membrane contactor made of either a microporous nonwoven PP or a nanoporous PBI (Table 1). The membrane contactors were positioned on top of the PDA before the inoculation. Petri plates were parafilm-sealed and incubated for 21 days at  $25^\circ\text{C}$  in the dark.

### 4.3. Characterization

A TA Instruments Q5000 SA Dynamic Vapor Sorption Analyzer was used for TGA, which involved heating the sample at a rate of  $10^\circ\text{C min}^{-1}$  up to  $100^\circ\text{C}$ , an isotherm at  $100^\circ\text{C}$  for 20 min, and then a gradient of  $10^\circ\text{C min}^{-1}$  up to  $900^\circ\text{C}$ . For purging,





nitrogen was employed as a protective gas. Using a DSC250 equipment from TA Instruments, DSC was conducted at a nitrogen flow rate of 50 mL min<sup>-1</sup>, at a heating rate of 5 °C min<sup>-1</sup> from 50 °C to 200 °C, and at a cooling rate of 5 °C min<sup>-1</sup> from 200 °C to 50 °C. TRIOS software from TA Instruments was utilized for DSC data processing. Using a Thermo Scientific Nicolet iS10 Fourier-transform infrared (FTIR) spectrometer, the FTIR spectra of each sample were recorded.

The morphology of the fabricated membranes was examined using a scanning electron microscope (SEM) (Magellan SEM, FEI). Samples were placed in the Electron Microscopy Vacuum Cryo Manipulation System (EM VCM, Leica Microsystems) and plunge frozen in liquid nitrogen prior to analysis. They were then transferred *via* the Leica VCT500 shuttle under cryogenic temperature into the Leica ACE900, where they were automatically fractured, etched at -100 °C for 2 min, and then coated with 4 nm Pt. Fluorescence microscopy images were acquired using the Zeiss LSM 710 Confocal Microscope. Before analysis, materials were stained with a 1 mM Congo Red (SunYoung Chemical Ltd.) aqueous solution. WCA measurements were performed in triplicate on the membranes using the Young Laplace method and a KRÜSS Scientific Drop Shape Analyzer DSA100E. Tapping-mode AFM was used to describe the surface topographies of the membranes (Dimension Icon SPM, Bruker, RTESPA-300 probe).

#### 4.4. Oil separation

The membranes were divided into squares of 100 mm<sup>2</sup> size, and their dry weights were then measured. The membranes were immersed in 10 mL of oil–water mixtures containing crude oil, soybean oil, gasoline, olive oil, or diesel for 1, 10, 30, 60, or 720 min. After the membranes were taken out, their weight was once more measured in duplicate. The following equation was used to compute the oil sorption capacity:

$$c_{\text{sorp}} (\text{g g}^{-1}) = \frac{m_t - m_0}{m_0}, \quad (1)$$

where  $m_0$  and  $m_t$  are the masses of the sample before and after sorption, respectively. The oil–water selectivity ( $S$ ) for the sorption process was calculated using the following equation:

$$S = \frac{m_{\text{oil}}}{m_{\text{water}}}, \quad (2)$$

where  $m_{\text{oil}}$  is the mass (in grams) of oil adsorbed by the membrane and  $m_{\text{water}}$  is the mass (in grams) of water adsorbed by the membrane.

## Data availability

All data needed to evaluate the conclusions in the paper are present in the paper and/or the ESI. Additional data related to this paper can be requested from the authors.

## Authorship contribution

JC: conceptualization, methodology, data curation, investigation, visualization, writing: original draft; GS: conceptualization, resources, methodology, visualization, writing: review &

editing, supervision, funding acquisition, project administration.

## Conflicts of interest

The authors declare that they have no known competing financial interests or personal relationships that could have appeared to influence the work reported in this paper.

## Acknowledgements

The research reported in this publication was financially supported by the funding received from King Abdullah University of Science and Technology (KAUST). The graphical abstract and Fig. 1 were produced by Thom Leach, who is a scientific illustrator at KAUST.

## References

- 1 L. Yang, X. Shen, Q. Yang, J. Liu, W. Wu, D. Li, J. Du, B. Zhang and S. Fan, Fabrication of biomimetic anisotropic superhydrophobic surface with rice leaf-like structures by femtosecond laser, *Opt. Mater.*, 2021, **112**, 110740.
- 2 N. Ahmad, C. E. Wee, L. K. Wai, N. M. Zin and F. Azmi, Biomimetic amphiphilic chitosan nanoparticles: Synthesis, characterization and antimicrobial activity, *Carbohydr. Polym.*, 2021, **254**, 117299.
- 3 Y. Liu and M.-O. Coppens, Cell Membrane-Inspired Graphene Nanomesh Membrane for Fast Separation of Oil-in-Water Emulsions, *Adv. Funct. Mater.*, 2022, **32**, 2200199.
- 4 C. Zhang, Y. Zhang, X. Xiao, G. Liu, Z. Xu, B. Wang, C. Yu, R. H. A. Ras and L. Jiang, Efficient separation of immiscible oil/water mixtures using a perforated lotus leaf, *Green Chem.*, 2019, **21**, 6579–6584.
- 5 P. Yang, L. Xu, P. Trogadas, M.-O. Coppens and Y. Lan, Bioinspired supramolecular macrocycle hybrid membranes with enhanced proton conductivity, *Nano Res.*, 2023, **1**, 1–8.
- 6 W. Choi, C. Lee, D. Lee, Y. J. Won, G. W. Lee, M. G. Shin, B. Chun, T.-S. Kim, H.-D. Park, H. W. Jung, J. S. Lee and J.-H. Lee, Sharkskin-mimetic desalination membranes with ultralow biofouling, *J. Mater. Chem. A*, 2018, **6**, 23034–23045.
- 7 M. Afsari, H. K. Shon and L. D. Tijing, Janus membranes for membrane distillation: Recent advances and challenges, *Adv. Colloid Interface Sci.*, 2021, **289**, 102362.
- 8 I. Karapanagiotis and P. N. Manoudis, Superhydrophobic and superamphiphobic materials for the conservation of natural stone: An overview, *Constr. Build. Mater.*, 2022, **320**, 126175.
- 9 M. Fromel, D. M. Sweeder, S. Jang, T. A. Williams, S. H. Kim and C. W. Pester, Superhydrophilic Polymer Brushes with High Durability and Anti-fogging Activity, *ACS Appl. Polym. Mater.*, 2021, **3**, 5291–5301.
- 10 X. Cheng, Y. Ye, Z. Li, X. Chen, Q. Bai, K. Wang, Y. Zhang, E. Drioli and J. Ma, Constructing Environmental-Friendly “Oil-Diode” Janus Membrane for Oil/Water Separation, *ACS Nano*, 2022, **16**, 4684–4692.



- 11 Y. Saharan, J. Singh, R. Goyat, A. Umar, H. Algadi, A. A. Ibrahim, R. Kumar and S. Baskoutas, Nanoporous and hydrophobic new Chitosan-Silica blend aerogels for enhanced oil adsorption capacity, *J. Cleaner Prod.*, 2022, **351**, 131247.
- 12 U. Hwang, B. Lee, B. Oh, H. S. Shin, S. S. Lee, S. G. Kang, D. Kim, J. Park, S. Shin, J. Suhr, S.-H. Kim and J.-D. Nam, Hydrophobic lignin/polyurethane composite foam: An eco-friendly and easily reusable oil sorbent, *Eur. Polym. J.*, 2022, **165**, 110971.
- 13 N. M. Majib, S. T. Sam, N. D. Yaacob, N. M. Rohaizad and W. K. Tan, Characterization of Fungal Foams from Edible Mushrooms Using Different Agricultural Wastes as Substrates for Packaging Material, *Polymers*, 2023, **15**, 873.
- 14 X. Zhang, J. Hu, X. Fan and X. Yu, Naturally grown mycelium-composite as sustainable building insulation materials, *J. Cleaner Prod.*, 2022, **342**, 130784.
- 15 W. Aiduang, A. Chanthaluck, J. Kumla, K. Jatuwong, S. Srinuanpan, T. Waroonkun, R. Oranratmanee, S. Lumyong and N. Suwannarach, Amazing Fungi for Eco-Friendly Composite Materials: A Comprehensive Review, *J. Fungi*, 2022, **8**, 842.
- 16 M. Jones, A. Gandia, S. John and A. Bismarck, Leather-like material biofabrication using fungi, *Nat. Sustain.*, 2021, **4**, 9–16.
- 17 W. Sun, M. Tajvidi, C. G. Hunt and C. Howell, All-Natural Smart Mycelium Surface with Tunable Wettability, *ACS Appl. Bio Mater.*, 2021, **4**, 1015–1022.
- 18 M. B. Linder, G. R. Szilvay, T. Nakari-Setälä and M. E. Penttilä, Hydrophobins: the protein-amphiphiles of filamentous fungi, *FEMS Microbiol. Rev.*, 2005, **29**, 877–896.
- 19 F. Bajoul Kakahi, S. Ly, C. Tarayre, O. Deschaume, C. Bartic, P. Wagner, P. Compère, G. Derdelinckx, C. Blecker and F. Delvigne, Modulation of fungal biofilm physiology and secondary product formation based on physico-chemical surface properties, *Bioprocess Biosyst. Eng.*, 2019, **42**, 1935–1946.
- 20 A. Walther and A. H. E. Müller, Janus particles, *Soft Matter*, 2008, **4**, 663–668.
- 21 J. Raman, D.-S. Kim, H.-S. Kim, D.-S. Oh and H.-J. Shin, Mycofabrication of Mycelium-Based Leather from Brown-Rot Fungi, *J. Fungi*, 2022, **8**, 317.
- 22 S. Sivaprasad, S. K. Byju, C. Prajith, J. Shaju and C. R. Rejeesh, Development of a novel mycelium bio-composite material to substitute for polystyrene in packaging applications, *Mater. Today Proc.*, 2021, **47**, 5038–5044.
- 23 A. Javadian, H. L. Ferrand, D. E. Hebel and N. Saeidi, Application of Mycelium-Bound Composite Materials in Construction Industry: A Short Review, *SOJ Mater. Sci. Eng.*, 2020, **7**, 1–10.
- 24 A. Miao, M. Wei, F. Xu and Y. Wang, Influence of membrane hydrophilicity on water permeability: An experimental study bridging simulations, *J. Membr. Sci.*, 2020, **604**, 118087.
- 25 N. H. Ismail, W. N. W. Salleh, A. F. Ismail, H. Hasbullah, N. Yusof, F. Aziz and J. Jaafar, Hydrophilic polymer-based membrane for oily wastewater treatment: A review, *Sep. Purif. Technol.*, 2020, **233**, 116007.
- 26 G. Bekiaris, D. Tagkouli, G. Koutrotsios, N. Kalogeropoulos and G. I. Zervakis, Pleurotus Mushrooms Content in Glucans and Ergosterol Assessed by ATR-FTIR Spectroscopy and Multivariate Analysis, *Foods*, 2020, **9**, 535.
- 27 J. Hu, R. Hardian, M. Gede, T. Holtzl and G. Szekely, Reversible crosslinking of polybenzimidazole-based organic solvent nanofiltration membranes using difunctional organic acids: Toward sustainable crosslinking approaches, *J. Membr. Sci.*, 2022, **648**, 120383.
- 28 J. Cavalcante, R. Hardian and G. Szekely, Antipathogenic upcycling of face mask waste into separation materials using green solvents, *Sustainable Mater. Technol.*, 2022, **32**, e00448.
- 29 E. César, G. Canche-Escamilla, L. Montoya, A. Ramos, S. Duarte-Aranda and V. M. Bandala, Characterization and Physical Properties of Mycelium Films Obtained from Wild Fungi: Natural Materials for Potential Biotechnological Applications, *J. Polym. Environ.*, 2021, **29**, 4098–4105.
- 30 H. Yang, R. Yan, H. Chen, D. H. Lee and C. Zheng, Characteristics of hemicellulose, cellulose and lignin pyrolysis, *Fuel*, 2007, **86**, 1781–1788.
- 31 L. Paglia, V. Genova, M. P. Bracciale, C. Bartuli, F. Marra, M. Natali and G. Pulci, Thermochemical characterization of polybenzimidazole with and without nano-ZrO<sub>2</sub> for ablative materials application, *J. Therm. Anal. Calorim.*, 2020, **142**, 2149–2161.
- 32 S. Al-Amshawee, M. Y. B. M. Yunus, J. G. Lynam, W. H. Lee, F. Dai and I. H. Dakhil, Roughness and wettability of biofilm carriers: A systematic review, *Environ. Technol. Innovation*, 2021, **21**, 101233.
- 33 R. N. Wenzel, Resistance of Solid Surfaces to Wetting By Water, *Ind. Eng. Chem.*, 1936, **28**, 988–994.
- 34 A. B. D. Cassie and S. Baxter, Wettability of porous surfaces, *Trans. Faraday Soc.*, 1944, **40**, 546.
- 35 X. Wang and Q. Zhang, Role of surface roughness in the wettability, surface energy and flotation kinetics of calcite, *Powder Technol.*, 2020, **371**, 55–63.
- 36 L. Zhang, A. G. Zhou, B. R. Sun, K. S. Chen and H.-Z. Yu, Functional and versatile superhydrophobic coatings via stoichiometric silanization, *Nat. Commun.*, 2021, **12**, 982.
- 37 T. P. Rasitha, S. Sofia, B. Anandkumar and J. Philip, Long term antifouling performance of superhydrophobic surfaces in seawater environment: Effect of substrate material, hierarchical surface feature and surface chemistry, *Colloids Surf., A*, 2022, **647**, 129194.
- 38 R. Cai, K. Glinel, D. De Smet, M. Vanneste, N. Mannu, B. Kartheuser, B. Nysten and A. M. Jonas, Environmentally Friendly Super-Water-Repellent Fabrics Prepared from Water-Based Suspensions, *ACS Appl. Mater. Interfaces*, 2018, **10**, 15346–15351.
- 39 J. C. Petrucci, L. Tian and G. Barbastathis, The transport of intensity equation for optical path length recovery using partially coherent illumination, *Opt. Express*, 2013, **21**, 14430–14441.



- 40 X. Li, F. Wang, M. Liu and C. Dong, Hydrophobin CmHYD1 Is Involved in Conidiation, Infection and Primordium Formation, and Regulated by GATA Transcription Factor CmAreA in Edible Fungus, *Cordyceps militaris*, *J. Fungi*, 2021, **7**, 674.
- 41 M. Du, Y. Xie, M. Wang, H. Yang, B. Hu, I. Mukhtar, Y. Liu, Y. Tao, F. Liu and B. Xie, FFGA1 Protein Is Essential for Regulating Vegetative Growth, Cell Wall Integrity, and Protection against Stress in *Flammulina filiformis*, *J. Fungi*, 2022, **8**, 401.
- 42 S. S. Kulkarni, S. N. Nene and K. S. Joshi, Identification and characterization of a hydrophobin Vmh3 from *Pleurotus ostreatus*, *Protein Expression Purif.*, 2022, **195–196**, 106095.
- 43 B. Chen, T. Wada and H. Yabu, Amphiphilic Perforated Honeycomb Films for Gravimetric Liquid Separation, *Adv. Mater. Interfaces*, 2022, **9**, 2101954.
- 44 C. Yang, Z. Wang, M. Long, B. Qin, Y. Wang, K. Zhi, Y. Zheng, J. Zhao, W. Li, Z. Wang, M. Zhang, R. Zhang, H. Wu and Z. Jiang, Antifouling poly(phenylene sulfide) membrane with an amphiphilic surface for efficient oil/water separation, *J. Membr. Sci.*, 2023, **679**, 121690.
- 45 S. Yan, P. Jiang, X. Zhang, Y. Guo and W. Fang, Cryogenic efficient phase separation of oil–water emulsions with amphiphilic hyperbranched poly(amido-amine), *J. Mater. Chem. A*, 2023, **11**, 14145–14158.
- 46 C. Yu, J. Song, Z. Ma, J. Lu, W. Xing, M. Meng, J. Dai, Y. Yan and Y. Wu, Fabrication and evaluation of multilevel Janus-imprinted nanocomposite membranes through a connective method of dip-coating and delayed phase inversion for simultaneous adsorption and separation of tetrabromobisphenol A and cadmium ion, *Chem. Eng. J.*, 2022, **427**, 131610.
- 47 N. Haridharan, D. Sundar, L. Kurrupasamy, S. Anandan, C.-H. Liu and J. J. Wu, Oil spills adsorption and cleanup by polymeric materials: A review, *Polym. Adv. Technol.*, 2022, **33**, 1353–1384.
- 48 H. Kim, G. Zhang, T. C. M. Chung and C. Nam, A Role for Newly Developed Sorbents in Remediating Large-Scale Oil Spills: Reviewing Recent Advances and Beyond, *Adv. Sustainable Syst.*, 2022, **6**, 2100211.
- 49 I. B. Valtcheva, S. C. Kumbharkar, J. F. Kim, Y. Bhole and A. G. Livingston, Beyond polyimide: Crosslinked polybenzimidazole membranes for organic solvent nanofiltration (OSN) in harsh environments, *J. Membr. Sci.*, 2014, **457**, 62–72.
- 50 A. Asadi Tashvigh and T.-S. Chung, Robust polybenzimidazole (PBI) hollow fiber membranes for organic solvent nanofiltration, *J. Membr. Sci.*, 2019, **572**, 580–587.
- 51 K. Y. Wang, M. Weber and T.-S. Chung, Polybenzimidazoles (PBIs) and state-of-the-art PBI hollow fiber membranes for water, organic solvent and gas separations: a review, *J. Mater. Chem. A*, 2022, **10**, 8687–8718.
- 52 M. Osorio-Concepción, G. R. Cristóbal-Mondragón, B. Gutiérrez-Medina and S. Casas-Flores, Histone Deacetylase HDA-2 Regulates *Trichoderma atroviride* Growth, Conidiation, Blue Light Perception, and Oxidative Stress Responses, *Appl. Environ. Microbiol.*, 2017, **83**, 029222.

